

BUCKLING ANALYSIS OF THREE-LAYERED RECTANGULAR PLATE WITH PIEZOELECTRIC LAYERS

HESSAMEDDIN YAGHOOBI

Young Researchers and Elite Club, Central Tehran Branch, Islamic Azad University, Tehran, Iran
e-mail: yaghoobi.hessam@gmail.com

IRAJ RAJABI

K.N. Toosi University of Technology, Faculty of Mechanical Engineering, Tehran, Iran

This paper employs an analytical method to analyze the buckling of piezoelectric coupled plates with different boundary conditions on the basis of the first order shear deformation plate theory. The structure is composed of a host isotropic plate and two bonded piezoelectric layers. Convergence study is performed in order to verify the numerical stability of the presented method. Also, the present analysis is validated by comparing the results with those in the literature, and then the critical buckling load of the piezoelectric coupled plates is presented in tabular and graphical forms for different plate aspect ratios, thickness of the piezoelectric, actuator voltage and boundary conditions.

Key words: three-layered rectangular plate, piezoelectric, critical buckling load

1. Introduction

Piezoelectric materials have strongly attracted the attention of many research groups due to their unique electromechanical coupling characteristics which produce mechanical deformations under application of electrical loads and electrical fields under application of mechanical loads. The main advantages of these types of smart materials are high precision, low weight and high sensibility. Smart structures (e.g., piezoelectric coupled plates) may be used as sensors or/and actuators in various engineering applications including vibration control, acoustic noise suppression, active damping and so on. They are commonly used as an embedded layer on host structures. As a result, a thorough understanding of the interaction between the host structure and piezoelectric layer is helpful in order to effectively utilize this combination in different applications.

Shape or vibration control of laminated plates with integrated piezoelectric sensors and actuators has been identified as an important field of study in recent years. However, relatively few works have been done on the compressive and/or thermal buckling of plates containing piezoelectric layers. Oh *et al.* (2000) investigated postbuckling and vibration analysis considering large thermopiezoelectric deflections for fully symmetric and partially eccentric piezolaminated composite plates. The non-linear finite element equations based on the layerwise displacement theory were formulated for piezolaminated plates subject to thermal and piezoelectric loads. The Newton-Raphson iteration method was used to solve the non-linear equation. Shen (2001a,b) analyzed compressive and thermal postbuckling of shear deformable laminated plates with fully covered or embedded piezoelectric actuators subjected to combined mechanical, electrical and thermal loads. A higher order shear deformation plate theory was adopted and the initial geometric imperfection of plates was accounted. It was found that the control voltage had a small effect on the postbuckling load-deflection relationship of shear deformable piezolaminated plates with immovable unloaded edges, and almost no effect on the postbuckling load-deflection relationships of the same plate with movable edges.

Coupled multi-field generalized non-linear mechanics together with an associated plate finite element for analyzing the buckling and postbuckling response of active and sensory piezoelectric-composite laminated plates including non-linear effects due to large rotations and stress stiffening were presented by Varelis and Saravanos (2004). The discrete coupled equations of motion of the smart structure were finally linearized and solved using an incremental-iterative method based on the Newton-Raphson technique. Kapuria and Achary (2006, 2008) employed 3D elasticity and zigzag theory for linear compressive and thermal buckling of laminated plates containing piezoelectric layers. Akhras and Li (2008) extended the finite layer method to thermal buckling analysis of rectangular simply supported symmetrical cross-ply piezoelectric composite plates. Using this method, the three-dimensional analysis was transformed into one-dimensional analysis by virtue of the orthogonal properties of trigonometric interpolation functions.

Buckling optimization of laminated plates with integrated piezoelectric actuators can be found in Correia *et al.* (2003). Assessment of third order smeared and zigzag theories for buckling and vibration of symmetrically laminated hybrid angle-ply plates containing piezoelectric layers can be found in Dumir *et al.* (2009). Shariyat (2009) studied dynamic buckling of laminated plates with piezoelectric sensors and actuators under thermo-electro-mechanical loads using a finite element formulation based on a higher-order shear deformation theory. A nine-node second order Lagrangian element, an efficient numerical algorithm for solving the resulted highly non-linear governing equations, and an instability criterion already proposed by the author were employed. Shen and Zhu (2011) investigated compressive postbuckling under thermal environments and thermal postbuckling due to a uniform temperature rise for a shear deformable laminated plate with piezoelectric fiber reinforced composite (PFRC) actuators based on a higher order shear deformation plate theory that includes thermo-piezoelectric effects.

In the present research, buckling analysis of a three-layered rectangular plate with piezoelectric layers is investigated. Based on the first order shear deformation plate theory, the equilibrium and stability equations are obtained. Introducing a new analytical method, the coupled stability equations are converted into independent partial differential equations. It is assumed that the plate is simply supported on two opposite edges and has arbitrary boundary conditions along the other edges. By using the Levy solution, these equations are converted into two ordinary differential equations, one of which has variable coefficients. For solving the equations accurately, the power series method of Frobenius (see Wylie and Barrett, 1951) is used. To examine accuracy of the present formulation and procedure, several convergence and comparison studies are investigated. Also, the effects of some parameters of the plate and piezoelectric layers on the critical buckling load are studied.

2. Stability equations

Consider a three-layered rectangular plate, made of an isotropic substrate of thickness h and piezoelectric films of thickness h_a that are perfectly bonded on its top and bottom surfaces as actuators, as shown in Fig. 1. The length and the width of the plate are a and b , respectively. Rectangular Cartesian coordinates (x, y, z) are assumed for derivations in this study.

The displacement components of the plate based on the first-order shear deformation plate theory are considered as (Reddy, 1984, 2004)

$$\begin{aligned} u(x, y, z) &= u_0(x, y) + z\psi_x(x, y) & v(x, y, z) &= v_0(x, y) + z\psi_y(x, y) \\ w(x, y, z) &= w_0(x, y) \end{aligned} \quad (2.1)$$

where u , v and w represent the displacement of the plate in the x , y and z directions, respectively, u_0 and v_0 are the displacements of the mid-plane, w_0 is the transverse displacement, and ψ_x and ψ_y show rotation terms about y and x axes, respectively. The parameters u_0 , v_0 , w_0 ,

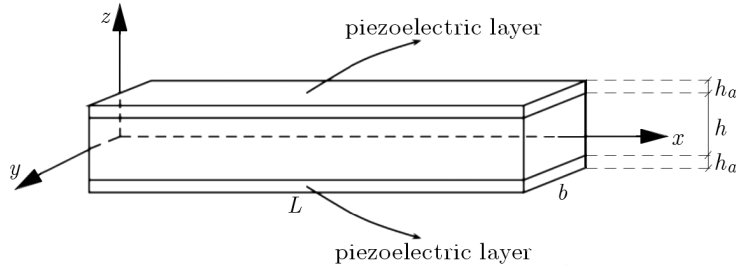


Fig. 1. Coordinate system and geometry of a rectangular plate integrated with piezoelectric layers

ψ_x and ψ_y are all functions of x and y variables. In this theory, the transverse normal do not remain perpendicular to the mid-surface after deformation. This amounts to including transverse shear strains in the theory. The inextensibility of the transverse normal requires that w not be a function of the thickness coordinate z (Reddy, 2004).

Using the non-linear form of strain-displacement relations, the following strain components are obtained (Reddy, 2004)

$$\begin{Bmatrix} \varepsilon_{xx} \\ \varepsilon_{yy} \\ \gamma_{yz} \\ \gamma_{xz} \\ \gamma_{xy} \end{Bmatrix} = \begin{Bmatrix} u_{,x} + w_{,x}^2/2 \\ v_{,y} + w_{,y}^2/2 \\ \psi_y + w_{,y} \\ \psi_x + w_{,x} \\ u_{,y} + v_{,x} + w_{,x}w_{,y} \end{Bmatrix} = \begin{Bmatrix} \varepsilon_{xx}^{(0)} \\ \varepsilon_{yy}^{(0)} \\ \gamma_{yz}^{(0)} \\ \gamma_{xz}^{(0)} \\ \gamma_{xy}^{(0)} \end{Bmatrix} + z \begin{Bmatrix} \varepsilon_{xx}^{(1)} \\ \varepsilon_{yy}^{(1)} \\ 0 \\ 0 \\ \gamma_{xy}^{(1)} \end{Bmatrix} \quad (2.2)$$

where

$$\begin{Bmatrix} \varepsilon_{xx}^{(0)} \\ \varepsilon_{yy}^{(0)} \\ \gamma_{yz}^{(0)} \\ \gamma_{xz}^{(0)} \\ \gamma_{xy}^{(0)} \end{Bmatrix} = \begin{Bmatrix} u_{0,x} + w_{0,x}^2/2 \\ v_{0,y} + w_{0,y}^2/2 \\ \psi_y + w_{0,y} \\ \psi_x + w_{0,x} \\ u_{0,y} + v_{0,x} + w_{0,x}w_{0,y} \end{Bmatrix} \quad \text{and} \quad \begin{Bmatrix} \varepsilon_{xx}^{(1)} \\ \varepsilon_{yy}^{(1)} \\ \gamma_{xy}^{(1)} \end{Bmatrix} = \begin{Bmatrix} \psi_{x,x} \\ \psi_{y,y} \\ \psi_{x,y} + \psi_{y,x} \end{Bmatrix} \quad (2.3)$$

Subscript $(,)$ denotes derivation with respect to the coordinates. The constitutive law for hybrid rectangular plates, taking into account the piezoelectric effect, is given by Liew *et al.* (2003)

$$\begin{Bmatrix} \sigma_{xx} \\ \sigma_{yy} \\ \tau_{yz} \\ \tau_{xz} \\ \tau_{xy} \end{Bmatrix} = \begin{bmatrix} Q_{11} & Q_{12} & 0 & 0 & 0 \\ Q_{21} & Q_{22} & 0 & 0 & 0 \\ 0 & 0 & Q_{44} & 0 & 0 \\ 0 & 0 & 0 & Q_{55} & 0 \\ 0 & 0 & 0 & 0 & Q_{66} \end{bmatrix} \begin{Bmatrix} \varepsilon_{xx} \\ \varepsilon_{yy} \\ \gamma_{yz} \\ \gamma_{xz} \\ \gamma_{xy} \end{Bmatrix} - \begin{bmatrix} 0 & 0 & e_{31} \\ 0 & 0 & e_{32} \\ 0 & 0 & 0 \\ 0 & e_{24} & 0 \\ e_{15} & 0 & 0 \end{bmatrix} \begin{Bmatrix} E_x \\ E_y \\ E_z \end{Bmatrix} \quad (2.4)$$

where Q_{ij} ($i, j = 1, \dots, 6$) is the elastic stiffness of the layers given by

$$Q_{11} = Q_{22} = \frac{E}{1 - \nu^2} \quad Q_{12} = Q_{21} = \frac{\nu E}{1 - \nu^2} \quad Q_{44} = Q_{55} = Q_{66} = \frac{E}{2(1 + \nu)} \quad (2.5)$$

The piezoelectric stiffness e_{31} , e_{32} , e_{15} and e_{24} can be expressed in terms of the dielectric constants d_{31} , d_{32} , d_{15} and d_{24} . The elastic stiffness Q_{ij}^a ($i, j = 1, \dots, 6$) of the piezoelectric actuator layers as

$$\begin{aligned} e_{31} &= (d_{31}Q_{11}^a + d_{32}Q_{21}^a) & e_{32} &= (d_{31}Q_{12}^a + d_{32}Q_{22}^a) \\ e_{24} &= d_{24}Q_{44}^a & e_{15} &= d_{15}Q_{55}^a \end{aligned} \quad (2.6)$$

As only the transverse electric field component E_z is dominant in the plate type piezoelectric material, it is assumed that

$$\begin{pmatrix} E_x \\ E_y \\ E_z \end{pmatrix} = \begin{pmatrix} 0 \\ 0 \\ V_a/h_a \end{pmatrix} \quad (2.7)$$

where V_a is the voltage applied to the actuators in the thickness direction.

The equilibrium equations under mechanical load may be derived on the basis of the stationary potential energy. The equilibrium equations of a plate can be obtained using the principle of minimum total potential energy (Reddy, 1984)

$$\begin{aligned} N_{xx,x} + N_{xy,y} &= 0 & N_{xy,x} + N_{yy,y} &= 0 \\ M_{xx,x} + M_{xy,y} - Q_{xz} &= 0 & M_{xy,x} + M_{yy,y} - Q_{yz} &= 0 \\ N_{xx}w_{,xx} + 2N_{xy}w_{,xy} + N_{yy}w_{,yy} + Q_{xz,x} + Q_{yz,y} &= 0 \end{aligned} \quad (2.8)$$

Equations (2.8) are non-linear equilibrium equations based on the first-order shear deformation plate theory. In Eqs. (2.8), the terms N , Q and M are stress and moment resultants. Using the constitutive relations, the stress and moment resultants are defined as

$$\begin{aligned} N_{xx} &= \int_{-\frac{h}{2}-h_a}^{\frac{h}{2}+h_a} \sigma_{xx} dz = A_1\varepsilon_{xx}^{(0)} + A_3\varepsilon_{yy}^{(0)} + B_1\psi_{x,x} + B_3\psi_{y,y} - 2V_a(d_{31}Q_{11}^a + d_{32}Q_{21}^a) \\ N_{yy} &= \int_{-\frac{h}{2}-h_a}^{\frac{h}{2}+h_a} \sigma_{yy} dz = A_3\varepsilon_{xx}^{(0)} + A_1\varepsilon_{yy}^{(0)} + B_3\psi_{x,x} + B_1\psi_{y,y} - 2V_a(d_{31}Q_{12}^a + d_{32}Q_{22}^a) \\ N_{xy} &= \int_{-\frac{h}{2}-h_a}^{\frac{h}{2}+h_a} \sigma_{xy} dz = A_2\gamma_{xy}^{(0)} + B_2\gamma_{xy}^{(1)} \\ Q_{xz} &= k^2 \int_{-\frac{h}{2}-h_a}^{\frac{h}{2}+h_a} \sigma_{xz} dz = C\gamma_{xz}^{(0)} & Q_{yz} &= k^2 \int_{-\frac{h}{2}-h_a}^{\frac{h}{2}+h_a} \sigma_{yz} dz = C\gamma_{yz}^{(0)} \\ M_{xx} &= \int_{-\frac{h}{2}-h_a}^{\frac{h}{2}+h_a} \sigma_{xx}z dz = B_1\varepsilon_{xx}^{(0)} + B_3\varepsilon_{yy}^{(0)} + D_1\psi_{x,x} + D_3\psi_{y,y} \\ M_{yy} &= \int_{-\frac{h}{2}-h_a}^{\frac{h}{2}+h_a} \sigma_{yy}z dz = B_3\varepsilon_{xx}^{(0)} + B_1\varepsilon_{yy}^{(0)} + D_3\psi_{x,x} + D_1\psi_{y,y} \\ M_{xy} &= \int_{-\frac{h}{2}-h_a}^{\frac{h}{2}+h_a} \sigma_{xy}z dz = B_2\gamma_{xy}^{(0)} + D_2\gamma_{xy}^{(1)} \end{aligned} \quad (2.9)$$

where the constants A_i , B_i , D_i , T_i , C in Eqs. (2.9) are

$$\begin{aligned}
(A_1, B_1, D_1) &= \int_{-\frac{h}{2}-h_a}^{\frac{h}{2}+h_a} Q_{11}(1, z, z^2) dz & (A_2, B_2, D_2) &= \int_{-\frac{h}{2}-h_a}^{\frac{h}{2}+h_a} Q_{44}(1, z, z^2) dz \\
(A_3, B_3, D_3) &= \int_{-\frac{h}{2}-h_a}^{\frac{h}{2}+h_a} Q_{12}(1, z, z^2) dz & C &= k^2 \int_{-\frac{h}{2}-h_a}^{\frac{h}{2}+h_a} Q_{44}(1, z, z^2) dz
\end{aligned} \tag{2.10}$$

In Eq. (2.10)₄, k^2 is the shear correction factor. Equations (2.8) are five coupled equilibrium equations, which are non-linear in terms of the displacement components. In order to obtain the stability equations, the adjacent equilibrium criterion is used (Brush and Almroth, 1975), and the stability equations are obtained as

$$\begin{aligned}
N_{xx,x}^1 + N_{xy,y}^1 &= 0 & N_{xy,x}^1 + N_{yy,y}^1 &= 0 \\
M_{xx,x}^1 + M_{xy,y}^1 - Q_{xz}^1 &= 0 & M_{xy,x}^1 + M_{yy,y}^1 - Q_{yz}^1 &= 0 \\
N_{xx}^0 w_{,xx}^1 + 2N_{xy}^0 w_{,xy}^1 + N_{yy}^0 w_{,yy}^1 + Q_{xz,x}^1 + Q_{yz,y}^1 &= 0
\end{aligned} \tag{2.11}$$

where N_{xx}^0 , N_{xy}^0 and N_{yy}^0 are the pre-buckling force resultants.

3. Decoupling the stability equations

In order to obtain the governing equations, the equivalent form of Eqs. (2.9) in terms of neighboring state displacements is substituted into Eqs. (2.11). Therefore, the stability equations in terms of the displacement components are obtained as follows

$$\begin{aligned}
A_2(u_{0,yy}^1 + v_{0,xy}^1) + B_2(\psi_{x,yy}^1 + \psi_{y,xy}^1) + A_3v_{0,xy}^1 + A_1u_{0,xx}^1 + B_3\psi_{y,xy}^1 + B_1\psi_{x,xx}^1 &= 0 \\
A_2(u_{0,xy}^1 + v_{0,xx}^1) + B_2(\psi_{x,xy}^1 + \psi_{y,xx}^1) + A_3u_{0,xy}^1 + A_1v_{0,yy}^1 + B_3\psi_{x,xy}^1 + B_1\psi_{y,yy}^1 &= 0 \\
B_1u_{0,xx}^1 + B_3v_{0,xy}^1 + D_1\psi_{x,xx}^1 + D_3\psi_{y,xy}^1 + B_2(u_{0,yy}^1 + v_{0,xy}^1) + D_2(\psi_{x,yy}^1 + \psi_{y,xy}^1) \\
- C(\psi_x^1 + w_{0,x}^1) &= 0 \\
B_2(u_{0,xy}^1 + v_{0,xx}^1) + D_2(\psi_{x,xy}^1 + \psi_{y,xx}^1) + B_3u_{0,xy}^1 + B_1v_{0,yy}^1 + D_3\psi_{x,xy}^1 + D_1\psi_{y,yy}^1 \\
- C(\psi_y^1 + w_{0,y}^1) &= 0 \\
N_{xx}^0 w_{0,xx}^1 + 2N_{xy}^0 w_{0,xy}^1 + N_{yy}^0 w_{0,yy}^1 + C(\psi_{x,x}^1 + w_{0,xx}^1) + C(\psi_{y,y}^1 + w_{0,yy}^1) &= 0
\end{aligned} \tag{3.1}$$

Based on Eqs. (2.10), the coefficients A_3 , B_3 and D_3 can be rewritten as

$$(A_3, B_3, D_3) = (A_1, B_1, D_1) - 2(A_2, B_2, D_2) \tag{3.2}$$

Equations (3.1) are five coupled equations in terms of the neighboring displacement components. To decouple governing stability equations (3.1), four new functions are introduced as

$$\varphi_1 = u_{0,x}^1 + v_{0,y}^1 \quad \varphi_2 = u_{0,y}^1 - v_{0,x}^1 \quad \varphi_3 = \psi_{x,x}^1 + \psi_{y,y}^1 \quad \varphi_4 = \psi_{x,y}^1 - \psi_{y,x}^1 \tag{3.3}$$

Using the functions introduced in relations (3.3), the stability Eqs. (3.1) can be expressed as

$$A_1\varphi_{1,x} + B_1\varphi_{3,x} + A_2\varphi_{2,y} + B_2\varphi_{4,y} = 0 \quad A_1\varphi_{1,y} + B_1\varphi_{3,y} - A_2\varphi_{2,x} - B_2\varphi_{4,x} = 0 \tag{3.4}$$

and

$$\begin{aligned}
B_1\varphi_{1,x} + D_1\varphi_{3,x} + B_2\varphi_{2,y} + D_2\varphi_{4,y} - k^2 A_2(\psi_x^1 + w_{0,x}^1) &= 0 \\
B_1\varphi_{1,y} + D_1\varphi_{3,y} - B_2\varphi_{2,x} - D_2\varphi_{4,x} - k^2 A_2(\psi_y^1 + w_{0,y}^1) &= 0
\end{aligned} \tag{3.5}$$

and

$$k^2 A_2(\varphi_3 + \nabla^2 w_0^1) + N_{xx}^0 w_{0,xx}^1 + 2N_{xy}^0 w_{0,xy}^1 + N_{yy}^0 w_{0,yy}^1 = 0 \quad (3.6)$$

where ∇^2 is the two-dimensional Laplace operator. It should be pointed out that the coefficients B_1 and B_2 are exactly equal to zero when the laminated plate is symmetric. By differentiation of Eqs. (3.5) with respect to the variables x and y , respectively, and simplifying the resulting equations, the function φ_3 is related to the transverse displacement w as follows

$$D_1 \nabla^2 \varphi_3 - k^2 A_2(\varphi_3 + \nabla^2 w_0^1) = 0 \quad (3.7)$$

From Eq. (3.6), φ_3 can be obtained as

$$\varphi_3 = -\frac{1}{k^2 A_2}(N_{xx}^0 w_{0,xx}^1 + 2N_{xy}^0 w_{0,xy}^1 + N_{yy}^0 w_{0,yy}^1) - \nabla^2 w_0^1 \quad (3.8)$$

Substituting Eq. (3.8) into Eq. (3.7) yields

$$\begin{aligned} & -\frac{D_1}{k^2 A_2} \nabla^2 (N_{xx}^0 w_{0,xx}^1 + 2N_{xy}^0 w_{0,xy}^1 + N_{yy}^0 w_{0,yy}^1) - D_1 \nabla^2 \nabla^2 w_0^1 \\ & + (N_{xx}^0 w_{0,xx}^1 + 2N_{xy}^0 w_{0,xy}^1 + N_{yy}^0 w_{0,yy}^1) = 0 \end{aligned} \quad (3.9)$$

Following the same procedure as was done to formulate Eq. (3.9), the following equation can be obtained in terms of function φ_4 as follows

$$D_2 \nabla^2 \varphi_4 - k^2 A_2 \varphi_4 = 0 \quad (3.10)$$

Equations (3.9) and (3.10) are two decoupled equations in terms of the transverse displacement w_0 and function φ_4 , respectively. Using Eqs. (3.5), and (3.8), the rotation functions ψ_x and ψ_y can be expressed in terms of w_0 and φ_4 as

$$\begin{aligned} \psi_x^1 &= \frac{D_1}{k^2 A_2} \left[-\frac{k^2 A_2}{D_1} w_0^1 - \frac{1}{k^2 A_2} (N_{xx}^0 w_{0,xx}^1 + 2N_{xy}^0 w_{0,xy}^1 + N_{yy}^0 w_{0,yy}^1) - \nabla^2 w_0^1 \right]_{,x} + \frac{D_2}{k^2 A_2} \varphi_{4,y} \\ \psi_y^1 &= \frac{D_1}{k^2 A_2} \left[-\frac{k^2 A_2}{D_1} w_0^1 - \frac{1}{k^2 A_2} (N_{xx}^0 w_{0,xx}^1 + 2N_{xy}^0 w_{0,xy}^1 + N_{yy}^0 w_{0,yy}^1) - \nabla^2 w_0^1 \right]_{,y} - \frac{D_2}{k^2 A_2} \varphi_{4,x} \end{aligned} \quad (3.11)$$

4. Boundary conditions

It is assumed that two opposite edges of the plate at $x = 0$ and $x = a$ are simply supported (S) and have arbitrary boundary conditions at the other two edges. The arbitrary boundary conditions along the other edges, $y = 0$ and $y = b$ can be clamped-clamped (CC), free-free (FF), simply supported-simply supported (SS), free-clamped (FC), free-simply supported (FS) and clamped-simply supported (CS). Each boundary may have the following conditions:

— Simply Supported

$$v_0 = w_0 = \psi_x = 0 \quad (4.1)$$

— Clamped

$$w_0 = \psi_x = \psi_y = 0 \quad (4.2)$$

— Free

$$M_{yy} = M_{xy} = Q_{yz} + N_{xy}^0 w_{0,x}^1 + N_{yy}^0 w_{0,y}^1 = 0 \quad (4.3)$$

The stress and moment resultants Q_{yz} , M_{yy} and M_{xy} can be defined as

$$\begin{aligned} M_{yy} &= D_1(\psi_{x,x} + \psi_{y,y}) - 2D_2\psi_{x,x} & M_{xy} &= D_2(\psi_{x,y} + \psi_{y,x}) \\ Q_{yz} &= k^2 A_2(\psi_y + w_{0,y}) \end{aligned} \quad (4.4)$$

which are functions of the rotation functions ψ_x and ψ_y and the transverse displacement w_0 .

5. Buckling analysis

To find the critical buckling load, the pre-buckling forces should be found. Thus, using the same procedure developed by Duc and Tung (2010), the pre-buckling force resultants are found to be

$$\begin{aligned} N_{xx}^0 &= -\frac{P_x}{b} & N_{xy}^0 &= 0 \\ N_{yy}^0 &= -\frac{A_3 P_x}{A_1 b} + \frac{A_1 - A_3}{A_1} [-2V_a(d_{31}Q_{12}^a + d_{32}Q_{22}^a)] \end{aligned} \quad (5.1)$$

where P_x is the uniformly distributed load along the edges $x = 0, a$. Substituting relations (5.1) into Eq. (3.9), yields

$$\begin{aligned} &-D_1 \nabla^2 \nabla^2 w_0^1 - \frac{D_1}{k^2 A_2} \nabla^2 \left[-\frac{P_x}{b} w_{0,xx}^1 \right. \\ &\quad \left. + \left(-\frac{A_3 P_x}{A_1 b} + \frac{A_1 - A_3}{A_1} [-2V_a(d_{31}Q_{12}^a + d_{32}Q_{22}^a)] \right) w_{0,yy}^1 \right] \\ &\quad \left. + \left[-\frac{P_x}{b} w_{0,xx}^1 + \left(-\frac{A_3 P_x}{A_1 b} + \frac{A_1 - A_3}{A_1} [-2V_a(d_{31}Q_{12}^a + d_{32}Q_{22}^a)] \right) w_{0,yy}^1 \right] = 0 \end{aligned} \quad (5.2)$$

To analyze the buckling behavior, decoupled stability equations (3.10) and (5.2) should be solved. As mentioned before, the edges of the plate in the x direction are assumed to be simply supported. Using the series solutions in the x direction, the functions w_0^1 and φ_4 are expressed as

$$w_0^1 = \sum_{m=1}^{\infty} f(y) \sin \frac{m\pi x}{a} \quad \varphi_4 = \sum_{m=1}^{\infty} g(y) \cos \frac{m\pi x}{a} \quad (5.3)$$

where m is the number of half-waves in the x direction. Series solutions (5.3) satisfy the simply supported boundary conditions in the x direction. Substituting relation (5.3) into Eqs. (3.10) and (5.2), yields two ordinary differential equations in terms of the functions $f(y)$ and $g(y)$ as follows

$$\begin{aligned} &D_1 \left(-\frac{A_3 P_x}{A_1 b} + \frac{A_1 - A_3}{A_1} [-2V_a(d_{31}Q_{12}^a + d_{32}Q_{22}^a)] + k^2 A_2 \right) \frac{d^4 f(y)}{dy^4} \\ &\quad + \left\{ -2D_1 \left(\frac{m\pi}{a} \right)^2 \left[-\frac{1}{2} \frac{P_x}{b} + k^2 A_2 + \frac{1}{2} \left(-\frac{A_3 P_x}{A_1 b} + \frac{A_1 - A_3}{A_1} [-2V_a(d_{31}Q_{12}^a + d_{32}Q_{22}^a)] \right) \right] \right. \\ &\quad \left. - k^2 A_2 \left(-\frac{A_3 P_x}{A_1 b} + \frac{A_1 - A_3}{A_1} [-2V_a(d_{31}Q_{12}^a + d_{32}Q_{22}^a)] \right) \right\} \frac{d^2 f(y)}{dy^2} \\ &\quad + \left[D_1 \left(\frac{m\pi}{a} \right)^4 \left(-\frac{P_x}{b} + k^2 A_2 \right) - \left(\frac{m\pi}{a} \right)^2 k^2 A_2 \frac{P_x}{b} \right] f(y) = 0 \\ &D_2 \left[-g(y) \left(\frac{m\pi}{a} \right)^2 + \frac{d^2 g(y)}{dy^2} \right] - k^2 A_2 g(y) = 0 \end{aligned} \quad (5.4)$$

Equation (5.4)₁ is an ordinary differential equation with variable coefficients. In order to solve this equation, the power series solution method of Frobenius (Wylie and Barrett, 1951) is utilized. To this end, the function $f(y)$ is written in the following form

$$f(y) = \sum_{j=0}^{\infty} C_j y^j \quad (5.5)$$

where C_j are arbitrary constant coefficients. Substituting proposed solution (5.5) into Eq. (5.4)₁, and shifting the indices, yields

$$\begin{aligned} & D_1 \left(-\frac{A_3 P_x}{A_1 b} + \frac{A_1 - A_3}{A_1} [-2V_a(d_{31}Q_{12}^a + d_{32}Q_{22}^a)] + k^2 A_2 \right) \\ & \cdot \sum_{j=0}^{\infty} [(j+4)(j+3)(j+2)(j+1)C_{j+4}y^j] + \left\{ -2D_1 \left(\frac{m\pi}{a} \right)^2 \left[-\frac{1}{2} \frac{P_x}{b} + k^2 A_2 \right. \right. \\ & \left. \left. + \frac{1}{2} \left(-\frac{A_3 P_x}{A_1 b} + \frac{A_1 - A_3}{A_1} [-2V_a(d_{31}Q_{12}^a + d_{32}Q_{22}^a)] \right) \right] \right. \\ & \left. - k^2 A_2 \left(-\frac{A_3 P_x}{A_1 b} + \frac{A_1 - A_3}{A_1} [-2V_a(d_{31}Q_{12}^a + d_{32}Q_{22}^a)] \right) \right\} \sum_{j=0}^{\infty} [(j+2)(j+1)C_{j+2}y^j] \\ & + \left[D_1 \left(\frac{m\pi}{a} \right)^4 \left(-\frac{P_x}{b} + k^2 A_2 \right) - \left(\frac{m\pi}{a} \right)^2 k^2 A_2 \frac{P_x}{b} \right] \sum_{j=0}^{\infty} (C_j y^j) = 0 \end{aligned} \quad (5.6)$$

Collecting the coefficients of similar powers of j in Eq. (5.6), from the coefficient of y^0 , it can be obtained

$$\begin{aligned} C_4 = & -\frac{1}{24D_1 \left(-\frac{A_3 P_x}{A_1 b} + \frac{A_1 - A_3}{A_1} [-2V_a(d_{31}Q_{12}^a + d_{32}Q_{22}^a)] + k^2 A_2 \right)} \\ & \cdot \left\{ \left[-2D_1 \left(\frac{m\pi}{a} \right)^2 \left[-\frac{1}{2} \frac{P_x}{b} + \frac{1}{2} \left(-\frac{A_3 P_x}{A_1 b} + \frac{A_1 - A_3}{A_1} [-2V_a(d_{31}Q_{12}^a + d_{32}Q_{22}^a)] \right) \right] + k^2 A_2 \right] \right. \\ & \left. - k^2 A_2 \left(-\frac{A_3 P_x}{A_1 b} + \frac{A_1 - A_3}{A_1} [-2V_a(d_{31}Q_{12}^a + d_{32}Q_{22}^a)] \right) \right\} C_2 \\ & + \left[D_1 \left(\frac{m\pi}{a} \right)^4 \left(-\frac{P_x}{b} + k^2 A_2 \right) - \left(\frac{m\pi}{a} \right)^2 k^2 A_2 \frac{P_x}{b} \right] C_0 \end{aligned} \quad (5.7)$$

Also, the coefficient of y^j gives

$$\begin{aligned} C_{j+4} = & -\frac{1}{D_1 \left(-\frac{A_3 P_x}{A_1 b} + \frac{A_1 - A_3}{A_1} [-2V_a(d_{31}Q_{12}^a + d_{32}Q_{22}^a)] + k^2 A_2 \right) (j+4)(j+3)(j+2)(j+1)} \\ & \cdot \left\{ \left[-2D_1 \left(\frac{m\pi}{a} \right)^2 \left(-\frac{1}{2} \frac{P_x}{b} + \frac{1}{2} \left(-\frac{A_3 P_x}{A_1 b} + \frac{A_1 - A_3}{A_1} [-2V_a(d_{31}Q_{12}^a + d_{32}Q_{22}^a)] \right) \right) \right] + k^2 A_2 \right] \\ & \left. - k^2 A_2 \left(-\frac{A_3 P_x}{A_1 b} + \frac{A_1 - A_3}{A_1} [-2V_a(d_{31}Q_{12}^a + d_{32}Q_{22}^a)] \right) \right\} (j+2)(j+1)C_{j+2} \\ & + \left[D_1 \left(\frac{m\pi}{a} \right)^4 \left(-\frac{P_x}{b} + k^2 A_2 \right) - \left(\frac{m\pi}{a} \right)^2 k^2 A_2 \frac{P_x}{b} \right] C_j \end{aligned} \quad (5.8)$$

Equations (5.7) and (5.8) are recursion relationships, and relation (5.8) is valid for $j \geq 0$. It should be noted that the coefficients C_i ($i = 0, 1, 2, 3$) are arbitrary coefficients on account of which the other coefficients C_j ($j \geq 4$) would be obtained just from recurrence formulas expressed in terms of them selves.

For solving Eq. (3.10), substituting proposed series solution (5.3)₂ into Eq. (3.10), and solving the resulted ordinary differential equation, yields

$$g(y) = C_{-1} \sinh(\lambda y) + C_{-2} \cosh(\lambda y) \quad (5.9)$$

where

$$\lambda = \sqrt{\left(\frac{m\pi}{a}\right)^2 + \frac{k^2 A_2}{D_2}} \quad (5.10)$$

Imposing the boundary conditions at the edges of the plate in the y direction, a system of six homogeneous algebraic equations is obtained. Setting the determinant of the coefficients equal to zero, the buckling load of the hybrid plate is determined. Needless to say that the lowest value among all of these P_x for each m is known as the critical buckling load P_{xcr} .

6. Results and discussion

Numerical results for buckling analysis of a three-layered rectangular plate with piezoelectric layers for different boundary conditions are computed. The material properties are shown in Table 1. This table shows the characteristics of PZT-5A as the piezoelectric and aluminum as the host plate. Moreover, for all numerical results which are reported here, the following values of variables are used unless otherwise indicated by tables or graphs

$$\frac{a}{b} = 1 \quad \frac{b}{t} = 100 \quad h_a = 0.001 \text{ m} \quad h = 0.01 \text{ m} \quad V_a = 500 \text{ V} \quad k^2 = \frac{5}{6}$$

Table 1. Material properties of the aluminum and PZT-5A layers

	Aluminum	PZT-5A
Elastic modulus E [GPa]	70	63
Poisson's ratio ν	0.3	0.3
Piezoelectric constant d_{31} [10^{-10} m/V]	–	2.54
Piezoelectric constant d_{32} [10^{-10} m/V]	–	2.54

In this Section, firstly, the convergence rate of the power series is checked. Secondly, comparison with the previously published related article is employed in order to verify the accuracy of the proposed method. Finally, the critical buckling load of the piezoelectric coupled plates are presented in tabular and graphical forms for different plate aspect ratios, thickness of piezoelectric, actuator voltage and boundary conditions.

To guarantee the accuracy of the buckling load obtained by the procedure described above, it is necessary to conduct a convergence study to determine the number of terms required in the power series solution. Since in real calculations a series solution will have to be truncated somewhere according to a pre-determined error bound, an exact solution really implies that the results can be obtained to any desired degree of accuracy. Therefore, the series expansion, Eq. (5.5), will have to be truncated in numerical calculations. Accordingly, to calculate a sufficient number of terms (N), a special case for all kinds of boundary conditions was studied.

Table 2 shows the convergence of P_{xcr} for six different boundary conditions. From this table, it is clearly visible that for the SSSS case, more than 18 terms are needed to obtain the value of P_{xcr} , accurately to six significant digits. Also, it is seen that if the SCSC is chosen as a boundary condition, at least 24 terms are required to obtain an extremely accurate value of P_{xcr} . The bold numbers in the table are those beyond which the sixth digit does not change as N

Table 2. Convergence test of the critical buckling load, P_{xcr} [KN], with different combinations of boundary conditions

N	Boundary conditions					
	SCSC	SSSC	SSSS	SFSC	SSSF	SFSF
10	423.4500	346.6509	251.0307	118.7528	108.3371	77.6299
12	551.1659	357.9866	253.8557	120.6816	106.5636	81.2094
14	524.5552	355.9793	253.5745	120.9698	106.2536	82.1316
16	530.1927	356.1081	253.5927	120.9983	106.2160	82.2540
18	529.9826	356.0962	253.5918	121.0004	106.2127	82.2646
20	530.0266	356.0965	253.5918	121.0005	106.2125	82.2653
22	530.0258	356.0965	253.5918	121.0005	106.2125	82.2653
24	530.0259	356.0965	253.5918	121.0005	106.2125	82.2653
26	530.0259	356.0965	253.5918	121.0005	106.2125	82.2653
28	530.0259	356.0965	253.5918	121.0005	106.2125	82.2653
30	530.0259	356.0965	253.5918	121.0005	106.2125	82.2653

increases. As more terms are taken, P_{xcr} converges to its exact value. Therefore, the numerical results from the power series approach which are presented in the calculations were obtained by taking sufficient terms N to converge to the number of digits shown in the tables.

In order to verify the accuracy of the present formulations, the buckling load obtained from the present method is compared with those available in the literature. In Table 3, comparison of the non-dimensional critical buckling loads for isotropic plates is made between the results obtained by the present method and those reported by Hosseini-Hashemi *et al.* (2008). For all boundary conditions, good agreements can be observed, and it is concluded that our formulation is completely trustful. After verifying the merit and accuracy of the present accurate solution, the following new results for the three-layered rectangular plate with piezoelectric actuators can be used as the benchmark for future research studies.

Table 3. Comparison of non-dimensional critical buckling loads ($P_{cr} = P_x a^2 / D_1$) for an isotropic rectangular plate with different boundary conditions for uniaxial compressive loading in the x direction

$\frac{a}{b}$	$\frac{h}{a}$		Boundary conditions					
			SCSC	SSSC	SSSS	SFSC	SSSF	SFSF
0.5	0.1	[6]	18.055467	16.247894	14.915722	10.642566	10.408425	9.325573
		Pr.	18.05546694	16.24789354	14.91572216	10.64256680	10.40842450	9.32557275
	0.2	[6]	15.851026	14.573567	13.580179	9.769217	9.590606	8.632796
		Pr.	15.85102641	14.57356705	13.58017889	9.76921715	9.59060641	8.63279575
1	0.1	[6]	63.404106	51.727083	37.447690	15.394207	13.257101	9.112050
		Pr.	63.40410565	51.72708294	37.44768979	15.39420741	13.25710052	9.11205022
	0.2	[6]	43.567623	41.394657	32.441432	13.627190	12.054586	8.434126
		Pr.	43.56762327	41.39465731	32.44143157	13.62719035	12.05458573	8.43412622
2	0.1	[6]	168.416063	151.127293	129.765726	46.387846	24.457914	8.891002
		Pr.	168.41606196	151.12729228	129.7657263	46.38784629	24.45791485	8.89100235
	0.2	[6]	80.032333	78.916068	76.902078	36.692284	21.430636	8.248819
		Pr.	80.03233149	78.91606516	76.90207522	36.69228453	21.43063569	8.24881884

[6] – Hosseini-Hashemi *et al.* (2008); Pr. – present

The variation of the critical buckling load versus the plate aspect ratio for three various voltage actuators are shown in Table 4 and Fig. 2. The primary conclusion tabulated from

Table 4 is that the critical buckling load diminishes as the plate aspect ratio increases. Moreover, the percentage decrease is about 89% for the SFSF plate and about 15% for the SCSC one from $a/b = 0.5$ to $a/b = 1.5$ under the same actuator voltage $V_a = -500$. It is worth mentioning that increasing the constraints on boundary conditions results in an increase in the critical buckling load, i.e. for a fixed value of variables, the SCSC and SFSF have the highest and lowest P_{xcr} , respectively. Figure 2 illustrates the effect of a/b for three various voltage actuators, i.e. 500, 0 and -500 on the P_{xcr} for the SFSC plate. It is apparent from this figure that the P_{xcr} can be increased by applying a negative voltage on the actuator layers, and the effect of V_a becomes more significant at higher plate aspect ratios.

Table 4. Effect of the plate aspect ratio on the critical buckling load for different boundary conditions

V_a	a/b	Boundary conditions					
		SCSC	SSSC	SSSS	SFSC	SSSF	SFSF
-500	0.5	620.6445	556.4839	511.1295	379.6773	371.7482	339.1097
	1.0	564.8202	389.0031	283.1340	135.4563	117.3006	82.9526
	1.5	525.5415	408.0511	270.2732	101.6814	72.9200	36.4562
0	0.5	615.4263	551.5939	506.6638	377.8521	370.1353	338.4924
	1.0	547.4352	372.5638	268.3629	128.3953	111.8539	82.6416
	1.5	514.6062	397.7806	244.4790	86.9342	61.9961	36.2055
+500	0.5	610.2019	546.6993	502.1981	375.9378	368.4899	337.9531
	1.0	530.0259	356.0965	253.5918	121.0005	106.2125	82.2653
	1.5	503.6551	387.4945	218.6847	71.3912	50.6116	35.8746

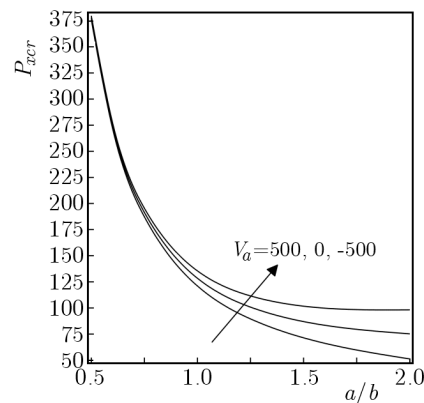


Fig. 2. Effect of the plate aspect ratio on the critical buckling load for the SFSC boundary condition

Figures 3a,b show the critical buckling load for hybrid laminated plates with different boundary conditions subjected to various actuator voltages. The results presented herein reveal that the minus actuator voltages increase the buckling load, whereas the plus actuator voltages decrease the buckling load at the same condition. Very high voltages will be able to influence the buckling response of the hybrid laminated plate. However, such high voltages cannot be applied, because they lead to breakdown in the material properties. It can also be seen from Fig. 3b that when the SFSF is chosen as a boundary condition, the effect of voltage actuator on the critical buckling load is very small. In Table 5, the effect of the ratio of the piezoelectric layer thickness to thickness of the host layer on the critical buckling load at different boundary conditions is tabulated. Also, in Fig. 4, this effect for the SSSS boundary condition is depicted. It is seen that with an increase in the piezo-to-host thickness ratio, the P_{xcr} increases.

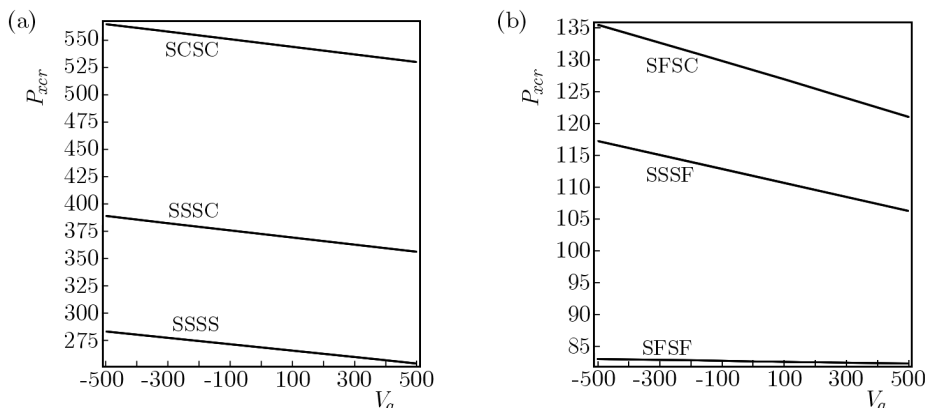


Fig. 3. Effect of the actuator voltage on the critical buckling load for the SCSC, SSSC and SSSS boundary conditions (a) and for the SFSC, SSSF and SFSF boundary conditions (b)

Table 5. Effect of the ratio of piezoelectric layer thickness to thickness of the host layer on the critical buckling load for different boundary conditions

h_a/h	Boundary conditions					
	SCSC	SSSC	SSSS	SFSC	SSSF	SFSF
0	382.3593	256.3732	182.2478	86.8944	76.3741	59.5945
0.1	530.0259	356.0965	253.5918	121.0005	106.2125	82.2653
0.2	708.1540	476.5520	339.8699	162.2539	142.2768	109.5356
0.3	916.0362	617.2578	440.7347	210.4871	184.4213	141.2979
0.4	1153.2794	777.9461	555.9935	265.6071	232.5654	177.4930

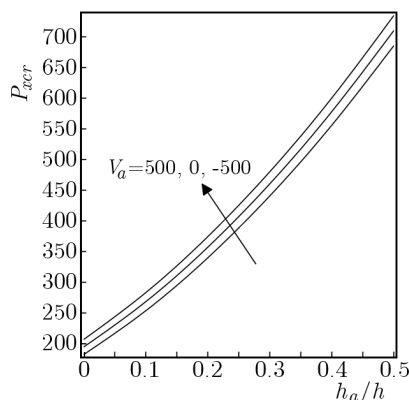


Fig. 4. Effect of the ratio of the piezoelectric layer thickness to thickness of the host layer on the critical buckling load for the SSSS boundary condition

7. Conclusion

In this article, mechanical buckling analysis has been presented for a three-layered rectangular plate with piezoelectric actuators subjected to the combined action of mechanical and electric loads. The derivations were based on the first-order plate theory and by employing an analytical approach, the five coupled governing stability equations are converted into two decoupled partial differential equations. By using the Levy solution, these equations are converted into two independent ordinary differential equations, and the power series method of Frobenius is used for solving these equations accurately. Extensive parametric studies for this structure under different sets of electric loading and boundary conditions have been carried out. The following conclusions, from the numerical computations were drawn.

- The buckling load is decreased by increasing the plate aspect ratio in both negative and positive actuator voltages and all boundary conditions.
- The application of negative voltage on the actuator layers can improve the mechanical buckling strength, and the critical buckling load can be controlled by applying a suitable voltage on the actuator layers.
- The critical buckling load increases with the increase of ratio of the piezoelectric layer thickness to the thickness of the host layer.
- Increasing the constraints on boundary conditions results in an increase in the critical buckling load.

References

1. AKHRAS G., LI W.C., 2008, Three-dimensional thermal buckling analysis of piezoelectric composite plates using the finite layer method, *Smart Materials and Structures*, **17**, 1-8
2. BRUSH D.O., ALMROTH B.O., 1975, *Buckling of Bars, Plates, and Shells*, McGraw-Hill, New York
3. CORREIA V.M.F., SOARES C.M.M., SOARES C.A.M., 2003, Buckling optimization of composite laminated adaptive structures, *Composite Structures*, **62**, 315-321
4. DUC N.D., TING H.V., 2010, Mechanical and thermal postbuckling of shear-deformable fgm plates with temperature-dependent properties, *Mechanics of Composite Materials*, **46**, 461-476
5. DUMIR P.C., KUMARI P., KAPURIA S., 2009, Assessment of third order smeared and zigzag theories for buckling and vibration of flat angle-ply hybrid piezoelectric panels, *Composite Structures*, **90**, 346-362
6. HOSSEINI-HASHEMI SH., KHORSHIDI K., AMABILI M., 2008, Exact solution for linear buckling of rectangular Mindlin plates, *Journal of Sound and Vibration*, **315**, 318-342
7. KAPURIA S., ACHARY G.G.S., 2004, Exact 3-D piezoelectricity solution for buckling of hybrid cross-ply plates using transfer matrices, *Acta Mechanica*, **170**, 25-45
8. KAPURIA S., ACHARY G.G.S., 2006, Nonlinear zigzag theory for electrothermomechanical buckling of piezoelectric composite and sandwich plates, *Acta Mechanica*, **184**, 61-76
9. LIEW K.M., YANG J., KITIPORNCHAI S., 2003, Postbuckling of piezoelectric FGM plates subject to thermo-electro mechanical loading, *International Journal of Solids and Structures*, **40**, 15, 3869-3892
10. OH K., HAN J.H., LEE I., 2000, Postbuckling and vibration characteristics of piezolaminated composite plate subject to thermopiezoelectric loads, *Journal of Sound and Vibration*, **233**, 1, 19-40
11. REDDY J.N., 1984, *Energy Principles and Variational Methods in Applied Mechanics*, John Wiley, New York
12. REDDY J.N., 2004, *Mechanics of Laminated Composite Plates and Shells: Theory and Analysis*, CRC Press LLC, USA
13. SHARIYAT M., 2009, Dynamic buckling of imperfect laminated plates with piezoelectric sensors and actuators subjected to thermo-electro-mechanical loadings, considering the temperature-dependency of the material properties, *Composite Structures*, **88**, 228-239
14. SHEN H.-S., 2001a, Postbuckling of shear deformable laminated plates with piezoelectric actuators under complex loading conditions, *International Journal of Solids and Structures*, **38**, 7703-7721
15. SHEN H.-S., 2001b, Thermal postbuckling of shear deformable laminated plates with piezoelectric actuators, *Composites Science and Technology*, **61**, 1931-1943

16. SHEN H.-S., ZHU Z.H., 2011, Compressive and thermal postbuckling behaviors of laminated plates with piezoelectric fiber reinforced composite actuators, *Applied Mathematical Modelling*, **35**, 1829-1845
17. VARELIS D., SARAVANOS D.A., 2004, Coupled buckling and postbuckling analysis of active laminated piezoelectric composite plates, *International Journal of Solids and Structures*, **41**, 1519-1538
18. WYLIE C.R., BARRETT L.C., 1951, *Advanced Engineering Mathematics*, New York, McGraw-Hill

Manuscript received September 14, 2012; accepted for print December 7, 2012